Supplementary Material

I. ADDITIONAL TR-ARPES DATA

In Fig. 2 of the main text we provide data for the p-doped sample at an excitation fluence of $1.5\,\mathrm{mJ/cm^2}$ and for the n-doped sample at an excitation fluence of $2.8\,\mathrm{mJ/cm^2}$. As discussed in detail below we expect the anisotropy to be fluence dependent. For a proper comparison between the two samples an excitation with the same fluence is desirable. In Fig. 1 we provide tr-ARPES data for the n-doped sample at an excitation fluence of $1.3\,\mathrm{mJ/cm^2}$, similar to the one for the p-doped sample in the main text. The reason why this data is not reported in the main text, is that in this measurement there is a time-zero drift between the data recorded with x- and y-polarized pump pulses, respectively, due to unstable air conditioning in the laboratory on that particular day. Due to this time-zero drift the anisotropy ΔN (obtained by subtracting the two data sets recorded with x- and y-polarized pump pulses for a given time delay, see Fig. 1b and c) cannot be determined properly. We want to stress that the difference between the two peak intensities in Fig. 1b is similar to the one in Fig. 2e of the main text where we show the tr-ARPES data for the n-doped sample for a higher pump fluence of $2.8\,\mathrm{mJ/cm^2}$. This indicates that increasing the pump fluence from 1.3 to $2.8\,\mathrm{mJ/cm^2}$ has a negligible effect on the amplitude of the measured anisotropy. This justifies the comparison made in Fig. 2 of the main text.

In Fig. 2 we present the hole dynamics in p- and n-doped samples in analogy to the electron dynamics in Fig. 2 in the main text. We find that the anisotropy of the holes is less pronounced than the one of the electrons for the n-doped sample. In the p-doped sample, we don't observe any anisotropy for electrons or holes.

II. MICROSCOPIC SIMULATIONS

Here, we present the theoretical study of the anisotropic carrier dynamics in graphene. The applied microscopic many-particle approach allows us to resolve the dynamics of optically excited electrons in time, energy, and momentum with respect to the polarization of the excitation pulse [1–3]. The core of the approach is built by Graphene Bloch Equations (GBE) that have been derived in the density matrix formalism within the second-order Born-Markov approximation [1, 4–8]. We obtain a system of coupled equations of motion for the carrier occupation $\rho^{\lambda}_{\mathbf{k}} = \langle a^{+}_{\lambda\mathbf{k}} a_{\lambda\mathbf{k}}\rangle$ in the state $(\mathbf{k},\lambda)$ characterized by the momentum $\mathbf{k}$ and the band index λ, the microscopic polarization $p_{\mathbf{k}} = \langle a^{+}_{v\mathbf{k}} a_{c\mathbf{k}}\rangle$ that is a measure for the transition probability between the valence ($\lambda = v$) and the conduction ($\lambda = c$) band, and phonon number $n^{j}_{\mathbf{q}} = \langle b^{+}_{j\mathbf{q}} b_{j\mathbf{q}}\rangle$ in the considered optical or acoustic phonon mode j with the phonon momentum $\mathbf{q}$. Here, we have expressed the microscopic quantities in the formalism of second quantization introducing creation and annihilation operators for electrons $(a^{+}_{\lambda\mathbf{k}}, a_{\lambda\mathbf{k}})$ and phonons $(b^{+}_{j\mathbf{q}}, b_{j\mathbf{q}})$ [9].

Applying the Heisenberg equation of motion and exploiting the fundamental commutation relations for fermions and bosons, we derive the GBE in second-order Born-Markov approximation yielding [1]

$$\dot{p}_{\mathbf{k}} = i\Delta\omega_{\mathbf{k}} p_{\mathbf{k}} - i\Omega^{vc}_{\mathbf{k}}\big(\rho^{c}_{\mathbf{k}} - \rho^{v}_{\mathbf{k}}\big) + \mathcal{U}_{\mathbf{k}} - \gamma_{\mathbf{k}} p_{\mathbf{k}}, \tag{1}$$

$$\dot{\rho}^{\lambda}_{\mathbf{k}} = \pm 2\mathrm{Im}\big(\Omega^{vc*}_{\mathbf{k}} p_{\mathbf{k}}\big) + \Gamma^{\mathrm{in}}_{\lambda,\mathbf{k}}\big(1+\rho^{\lambda}_{\mathbf{k}}\big) - \Gamma^{\mathrm{out}}_{\lambda,\mathbf{k}}\rho^{\lambda}_{\mathbf{k}}, \tag{2}$$

$$\dot{n}^{j}_{\mathbf{q}} = \Gamma^{\mathrm{em}}_{j,\mathbf{q}}\big(1+n^{j}_{\mathbf{q}}\big) - \Gamma^{\mathrm{abs}}_{j,\mathbf{q}} n^{j}_{\mathbf{q}} - \gamma_{j}\big(n^{j}_{\mathbf{q}} - n_{B}\big) \tag{3}$$

with the energy difference $\hbar\Delta\omega_{\mathbf{k}} = (E^{v}_{\mathbf{k}} - E^{c}_{\mathbf{k}})$, the Bose-Einstein distribution n_B denoting the equilibrium distribution of phonons, the phonon lifetime γ_j^{-1}, and the Rabi frequency $\Omega^{vc}_{\mathbf{k}}(t) = i\frac{e_0}{m_0}\mathbf{M}^{vc}_{\mathbf{k}}\cdot\mathbf{A}(t)$ describing the optical excitation of graphene with $\mathbf{M}^{vc}_{\mathbf{k}}$ as the optical matrix element [10, 11]. All quantities in GBE (except for n_B and $\Delta\omega_{\mathbf{k}}$) depend on time. The appearing matrix elements are calculated with tight-binding wave functions in the nearest-neighbor approximation [1], which is known to be a good approximation for graphene close to the Dirac point [12]. The doping is included via initial occupation of electrons and breaks the symmetry of the electron and hole dynamics [13]. The bare Coulomb potential $V(\mathbf{q})$ appearing in the Coulomb-induced scattering rates $\Gamma^{\mathrm{in/out}}_{\lambda,\mathbf{k}}(t)$ is screened due to the presence of many electrons and the substrate. The effects arising from the electrons in the core states and the surrounding subtrate are taken into account by introducing a dielectric background constant ε_{bg}. The screening stemming from other valence electrons are calculated within an effective single-particle Hamiltonian approach leading to the Lindhard approximation of the dielectric function $\varepsilon(\mathbf{q})$ [1, 5]. Since this many-particle-induced screening is directly influenced by carrier occupations in the conduction and valence bands, doping plays a crucial role and has a significant influence on the ultrafast carrier dynamics in graphene.

The equations take into account all relevant two-particle relaxation channels including Coulomb- and phonon-induced intra- and interband as well as intra- and intervalley scattering processes. The time- and momentum-dependent scattering rates $\Gamma_{\lambda\mathbf{k}}(t) = \Gamma^{\mathrm{c-c}}_{\lambda\mathbf{k}}(t) + \Gamma^{\mathrm{c-ph}}_{\lambda\mathbf{k}}(t)$ entering the equation for the carrier occupation $\rho^{\lambda}_{\mathbf{k}}(t)$ describe the strength of the carrier-carrier (c-c) and carrier-phonon (c-ph) scattering processes. For the phonon occupation, we obtain the corresponding emission and absorption rates $\Gamma^{\mathrm{em/abs}}_{j,\mathbf{q}}$ [14]. The many-particle scattering also contributes to diagonal ($\gamma_{\mathbf{k}}(t)$) and off-diagonal dephasing ($\mathcal{U}_{\mathbf{k}}(t)$) of the microscopic polarization $p_{\mathbf{k}}(t)$.

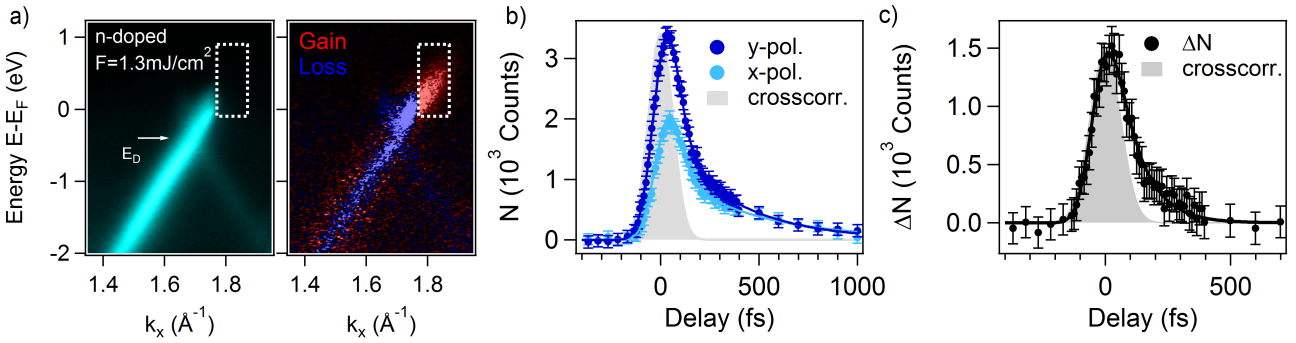

Figure 1. **Low-fluence tr-ARPES data for n-doped sample.** (a) Snapshot of the band structure at negative pump-probe delay together with pump-induced changes of the photocurrent at the time delay corresponding to the peak of the pump-probe signal for excitation with y-polarized light. (b) Intensity integrated over the area indicated by the white box in panel a for x- (light blue) and y-polarized pump pulses (dark blue) as a function of pump-probe delay. (c) Anisotropy ΔN given by the difference between the two curves in panel b. The grey-shaded area represents the temporal crosscorrelation between infrared pump and ultraviolet probe pulse.

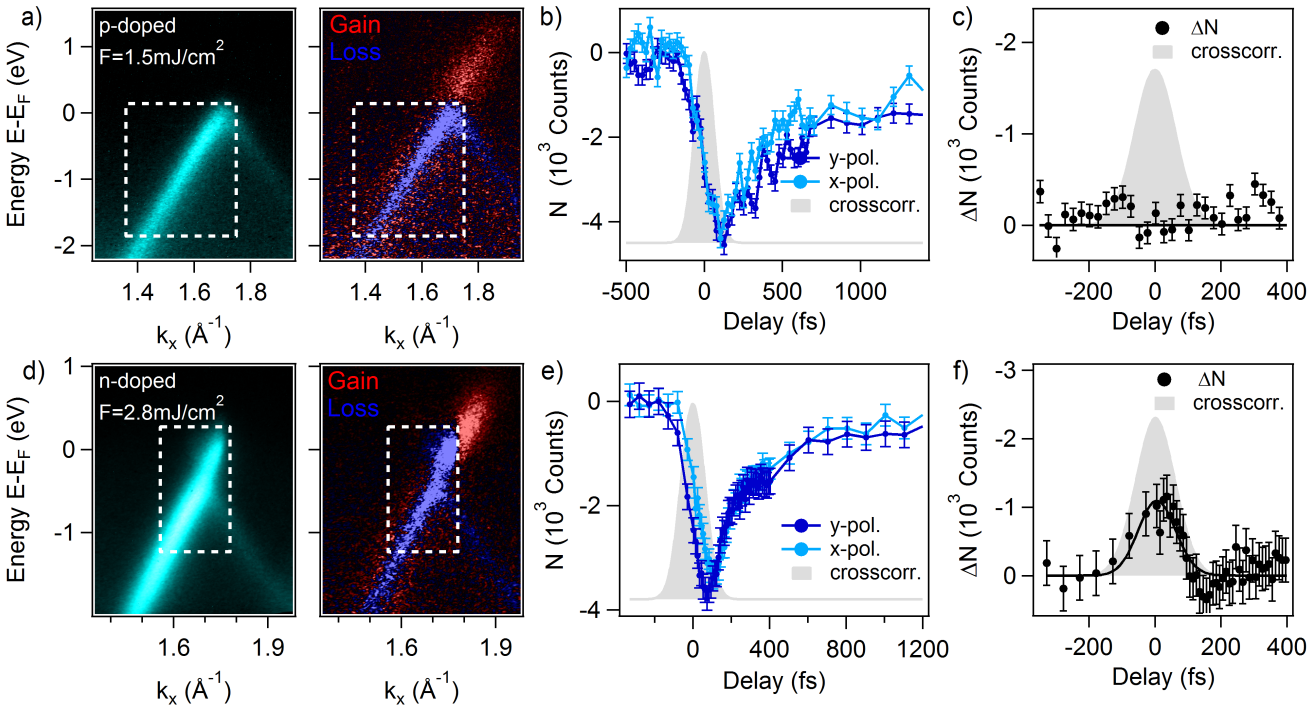

Figure 2. **Hole Dynamics.** Upper pannel: p-doped graphene, excitation fluence of 1.5 mJ/cm^2, lower panel: n-doped graphene, excitation fluence of 2.8 mJ/cm^2. a), d) ARPES spectra for negative time delays and pump-induced changes of the photocurrent for y-polarized pump pulses at the peak of the pump-probe signal. b), e) change of photocurrent integrated over the area of the white boxes in (a) and (d) versus pump-probe delay for x- (light blue) and y-polarized pump pulses (dark blue). The respective difference in intensity is shown in (c) and (f). The light gray area represents the temporal cross-correlation of pump and probe pulses.

More details on the theoretical approach can be found in Refs. [1, 2].

The aim of the current study is to model the measured anisotropy in tr-ARPES experiments on p- and n-doped graphene samples in the strong excitation regime. We investigate the anisotropy defined as

$$\Delta N = \frac{1}{\Delta E}\int_{E_F}^{E_{\max}} \left(\rho_E^{k_x}(t) - \rho_E^{k_y}(t)\right) dE, \qquad (4)$$

where $\rho_E^{k_x}(t)$ and $\rho_E^{k_y}(t)$ are the time-resolved carrier occupations evaluated in the direction (k_x) and opposite to

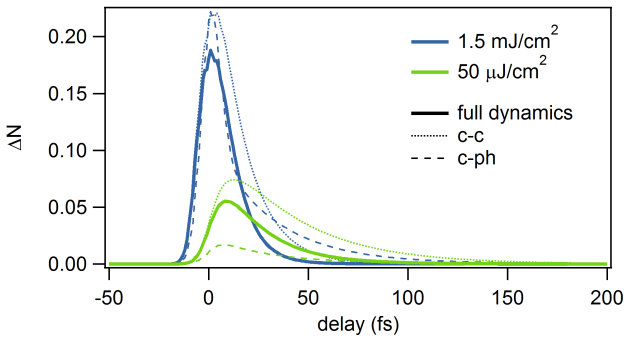

Figure 3. **Fluence dependence.** Temporal evolution of the carrier anisotropy ΔN (see Eq. 4) in an undoped graphene sample on SiC ($\varepsilon_s = 7.8$) for a relatively small ($50\,\mu$J/cm^2, green) and a relatively large pump fluence (1.5 mJ/cm^2, blue). To reveal the role of single many-particle processes, we show the full dynamics (continuous lines) and compare it with the dynamics taking into account only carrier-phonon scattering (dashed lines) and carrier-carrier scattering (dotted lines).

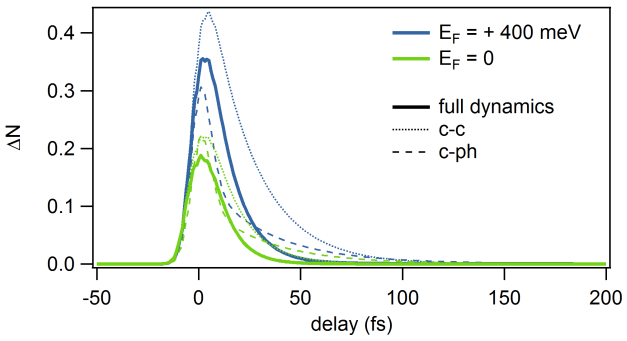

Figure 4. **Doping dependence.** Temporal evolution of the anisotropy ΔN in the strong excitation regime (1.5 mJ/cm^2) for n- (E_F=400 meV, blue) and undoped graphene (green) on SiC ($\varepsilon_s = 7.8$). The impact of Coulomb- (dotted line) and phonon-induced (dashed line) scattering channels is illustrated separately. The complete dynamics is shown as continuous lines.

the direction (k_y) of the polarization of the pump pulse. We integrate from the Fermi energy E_F up to a maximal energy well beyond the excitation energy to capture all of the photo-excited electrons. To get profound insights into the elementary processes behind the anisotropy, we investigate the impact of pump fluence, doping, and substrate screening on the anisotropy.

A. Impact of pump fluence

First, we focus on the dependence of the anisotropy on the applied pump fluence. We consider an undoped graphene sample on a SiC substrate with a dielectric constant of $\varepsilon_s = 7.8$ and directly compare the temporal evolution of the anisotropy for two different pump fluences ($50\,\mu$J/cm^2 and 1.5 mJ/cm^2, respectively) in Fig. 3. The large pump fluence is comparable to the one used in the tr-ARPES measurements in the main text. To reveal the elementary processes responsible for the decay of the anisotropy, we show the full dynamics (continuous lines) as well as calculations taking into account only carrier-phonon (c-ph, dashed lines) or carrier-carrier scattering (c-c, dotted lines). The most obvious impact of the fluence is a significantly increased anisotropy ΔN (see Eq. 4) in the strong excitation regime, simply reflecting the higher number of photo-excited carriers. Note that previous optical pump-probe measurements used a different definition for the anisotropy based on the pump-induced changes of the transmission ΔT. In this case, the ratio between ΔT for parallel and cross-polarized pump and probe beams was found to decrease with increasing fluence [15]. By comparing the dashed and dotted green lines in Fig. 4, we conclude that the decay of the anisotropy in the small fluence regime is dominated by c-ph scattering in good agreement with literature [2, 16, 17]. This is because optically excited carriers can efficiently scatter across the Dirac cone via different phonon modes. In contrast, Coulomb interaction prefers collinear scattering events [16–18]. The situation is different in the high fluence regime, where c-c becomes more efficient due to the large number of photo-excited electrons. In this case, non-collinear c-c scattering and c-ph scattering become of similar importance for the decay of the anisotropy (see the dotted and dashed blue lines in Fig. 3). However, c-ph scattering still remains the dominant channel for the reduction of the anistropy in the first tens of femtoseconds. Non-collinear c-c scattering becomes important at later times, where the dotted and dashed blue lines in Fig. 3 cross. This crossover happens once the photo-excited electrons, after having emitted a couple of phonons, are too close to the Fermi level to allow for further phonon emission.

B. Impact of doping

Now we study the influence of doping for a given fluence (1.5 mJ/cm^2) and substrate screening ($\varepsilon_s = 7.8$). We assume an n-doping of 400 meV, the same as in the tr-ARPES experiments. We find a bigger amplitude of the anisotropy in the n-doped graphene sample compared to the undoped graphene sample (blue and green in Fig. 4, respectively) for the full dynamics as well as for carrier-carrier and carrier-phonon scattering only. We attribute this to a combination of a reduced scattering phase space for c-c and c-ph scattering as well as a bigger screening of the Coulomb interaction due to the increased number of free carriers in the n-doped graphene sample.

C. Impact of substrate screening

In Fig. 5 we investigate the influence of the substrate on the amplitude and decay of the anisotropy of the photo-excited carrier distribution. The presence of a substrate can efficiently screen the Coulomb interaction by a factor of $1/\varepsilon_{\text{eff}}$, where $\varepsilon_{\text{eff}} = (1+\varepsilon_s)/2$ is related to the dielectric constant of the substrate ε_s [19]. We investigate the two substrates used in the tr-ARPES experiment: hydrogen-terminated SiC(0001) with a dielectric constant of $\varepsilon_s = 7.8$ (green in Fig. 5) and SiC(0001) covered by a $6\sqrt{3}$ carbon buffer layer with a dielectric constant of $\varepsilon_s = 43$ (blue in Fig. 5) [19]. We consider n-doped samples with E_F=400 meV in the strong excitation regime (1.5 mJ/cm^2). We find a considerably slower decay of the anisotropy for graphene on $6\sqrt{3}$ C-SiC exhibiting a large dielectric constant. This can be clearly ascribed to the drastically slower Coulomb-induced c-c scattering (see dotted lines in Fig. 5). In this situation, c-ph scattering becomes the dominant channel for redistributing the optically excited carriers and reducing the initial carrier anisotropy. Note that, in the framework of the present model, the c-ph coupling is unscreened.

D. Modelling of the measured anisotropy

Having understood the impact of pump fluence, doping, and substrate sceening, we now investigate the experimental conditions for the tr-ARPES measurements in the main part: an n-doped graphene sample on $6\sqrt{3}$ C-SiC (E_F=400 meV, $\varepsilon_s = 43$, blue in Fig. 6) and a p-doped graphene sample on H-SiC (E_F=-200 meV, $\varepsilon_s = 7.8$, green in Fig. 6) both excited with a strong pump fluence of 1.5 mJ/cm^2. In agreement with the experimental observations, we find a more pronounced and a longer-lived carrier anisotropy for the n-doped sample compared to the p-doped sample. This can be understood by a combination of doping (Fig. 4) and screening (Fig. 5): The higher the chemical potential μ_e, the smaller the scattering phase space for c-c and c-ph scattering. The larger the screening ε_s the slower the c-c scattering. Due to the large value of ε_s in the n-doped sample, the decay of the anisotropy is still dominated by c-ph scattering, even in the high fluence regime.

Finally, we separately study the temporal evolution of the electron anisotropy in the conduction band and the hole anisotropy in the valence band (Fig. 7). Due to the non-zero doping of our samples, the symmetry between electron and hole dynamics is broken. In good qualitative agreement with the experimental results, we find that the hole anisotropy is smaller and decays faster.

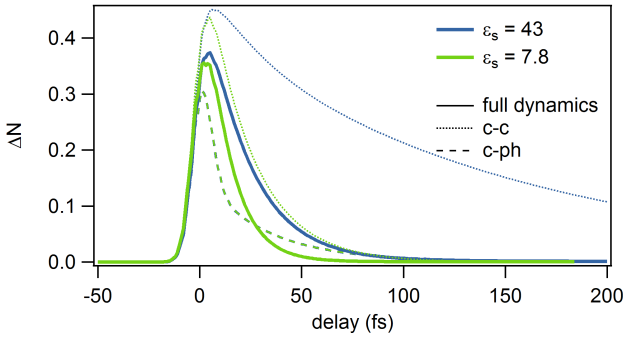

Figure 5. **Substrate dependence.** Temporal evolution of the carrier anisotropy ΔN in the strong excitation regime (1.5 mJ/cm^2) for an n-doped (E_F=400 meV) graphene sample on H-SiC (dielectric constant of $\varepsilon_s = 7.8$) and on $6\sqrt{3}$ C-SiC (dielectric constant of $\varepsilon_s = 43$). The continuous, dashed, and dotted lines represent the full dynamics, the dynamics with c-ph scattering only, and the dynamics with c-c scattering only, respectively. Note that the two dashed lines overlap.

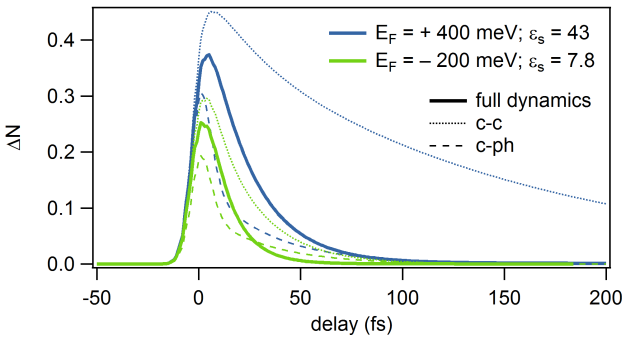

Figure 6. **tr-ARPES experiment.** Temporal evolution of the carrier anisotropy ΔN at the experimental conditions from the main text: n-doped (E_F=400 meV) graphene sample on $6\sqrt{3}$ C-SiC with a dielectric constant of $\varepsilon_s = 43$ (blue) in direct comparison to a p-doped (E_F=-200 meV) sample on H-SiC with a dielectric constant of $\varepsilon_s = 7.8$ (green) in the strong excitation regime (1.5 mJ/cm^2). The continuous, dashed, and dotted lines represent the full dynamics, the dynamics with c-ph scattering only, and the dynamics with c-c scattering only, respectively.

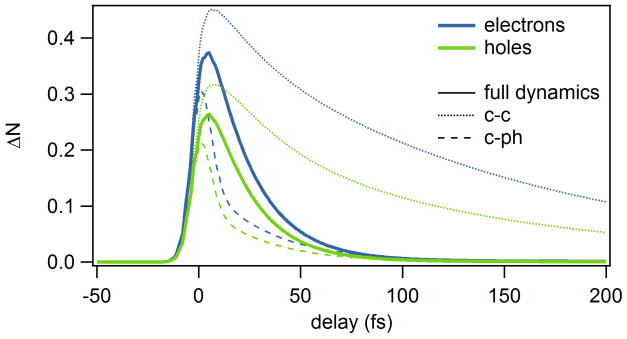

Figure 7. **Electron vs hole anisotropy.** Temporal evolution of the anisotropy ΔN for electrons (blue) and holes (green) under the experimental conditions from Fig. 6. The continuous, dashed, and dotted lines represent the full dynamics, the dynamics with c-ph scattering only, and the dynamics with c-c scattering only, respectively.

We attribute this to a smaller scattering phase space for c-c and c-ph scattering for the electrons in the conduction band compared to the holes in the valence band.

[1] E. Malić, and A. Knorr, Graphene and Carbon Nanotubes: Ultrafast Optics and Relaxation Dynamics, 1st ed. (Wiley-VCH, 2013)

[2] E. Malić, T. Winzer, E. Bobkin, and A. Knorr, Physical Review B 84, 205406 (2011)

[3] E. Malić, T. Winzer, F. Wendler, and A. Knorr, Microscopic view on ultrafast carrier dynamics in graphene, in Optical Properties of Graphene, ed. by R. Binder (World Scientific, 2016)

[4] M. Lindberg and S. W. Koch, Physical Review B 38, 3342 (1988)

[5] H. Haug and S. W. Koch, Quantum Theory of the Optical and Electronic Properties of Semiconductors (World Scientific, 2004)

[6] F. Rossi and T. Kuhn, Reviews of Modern Physics 74, 895 (2002)

[7] A. Knorr, S. Hughes, T. Stroucken, and S. W. Koch, Chemical Physics 210, 27 (1996)

[8] M. Kira and S. Koch, Progress in Quantum Electronics 30, 155 (2006)

[9] F. Kadi, T. Winzer, E. Malić, A. Knorr, F. Göttfert, M. Mittendorff, S. Winnerl, and M. Helm, Phys. Rev. Lett. 113, 035502 (2014)

[10] A. Grüneis, R. Saito, G. G. Samsonidze, T. Kimura, M. A. Pimenta, A. Jorio, A. G. SouzaFilho, G. Dresselhaus, and M. S. Dresselhaus, Phys. Rev. B 67, 165402 (2003)

[11] E. Malić, M. Hirtschulz, F. Milde, A. Knorr, and S. Reich, Physical Review B 74, 195431 (2006)

[12] S. Reich, J. Maultzsch, C. Thomsen, and P. Ordejón, Physical Review B 66, 035412 (2002)

[13] F. Kadi, T. Winzer, A. Knorr, and E. Malić, Sci. Rep. 5, 16841 (2015)

[14] E. Malić, C. Weber, M. Richter, V. Atalla, T. Klamroth, P. Saalfrank, S. Reich, and A. Knorr, Physical Review Letters 106, 097401 (2011)

[15] M. Trushin, A. Grupp, G. Soavi, A. Budweg, D. De Fazio, U. Sassi, A. Lombardo, A. C. Ferrari, W. Belzig, A. Leitenstorfer, and D. Brida, Phys. Rev. B 92, 165429 (2015)

[16] E. Malić, T. Winzer, and A. Knorr, Applied Physics Letters 101, 213110 (2012)

[17] M. Mittendorff, T. Winzer, E. Malić, A. Knorr, C. Berger, W. A. de Heer, H. Schneider, M. Helm, and S. Winnerl, Nano Letters 14, 1504 (2014)

[18] J. C. Koenig-Otto, M. Mittendorff, T. Winzer, E. Malić, A. Knorr, C. Berger, W. A. de Heer, A. Pashkin, H. Schneider, M. Helm, and S. Winnerl, Phys. Rev. Lett 117, 087401 (2016)

[19] A. L. Walter, A. Bostwick, K.-J. Jeon, F. Speck, M. Ostler, T. Seyller, L. Moreschini, Y. J. Chang, M. Polini, R. Asgari, A. H. MacDonald, K. Horn, and E. Rotenberg, Phys. Rev. B 84, 085410 (2011)